COMPUTER METHODS AND PROGRAMS IN BIOMEDICINE 111 (2013) 676–684

journal homepage: www.intl.elsevierhealth.com/journals/cmpb

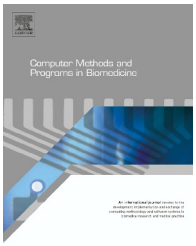

Use of shape-from-shading to estimate three-dimensional architecture in the small intestinal lumen of celiac and control patients

Edward J. Ciaccio[a,*], *Christina A. Tennyson*[a], *Govind Bhagat*[a,b], *Suzanne K. Lewis*[a], *Peter H.R. Green*[a]

[a] *Celiac Disease Center, Department of Medicine, Columbia University Medical Center, 180 Fort Washington Avenue, New York, NY 10032, USA*

[b] *Department of Pathology and Cell Biology, Columbia University Medical Center and New York Presbyterian Hospital, 630W 168th street, New York, NY 10032, USA*

ARTICLE INFO

Article history:
Received 20 March 2012
Received in revised form
18 May 2013
Accepted 6 June 2013

Keywords:
Celiac disease
Imaging
Shape-from-shading
Small intestine
Videocapsule

ABSTRACT

Background: As measured from videocapsule endoscopy images, the small intestinal mucosa of untreated celiac patients has significantly greater and more varied texture compared to normal patients. Three-dimensional modeling using shape-from-shading principles may further increase classification accuracy.

Methods: A sequence of 200 consecutive videocapsule images acquired at a $2\,s^{-1}$ frame rate and 576×576 pixel dimension, were obtained at four locations in the small intestinal lumen of ten patients with biopsy-proven celiac disease and ten control patients. Each two-dimensional image was converted to a three-dimensional architectural approximation by considering the 256 grayscale level to be linearly representative of image depth. From the resulting three-dimensional architecture, distinct luminal protrusions, representative of the macro-architecture, were automatically identified by computer algorithm. The range and number of protrusions per image, and their width and height, were determined for celiacs versus controls and tabulated as mean ± SD.

Results: The mean number of villous protrusions per image was 402.2 ± 15.0 in celiacs versus 420.8 ± 24.0 in controls ($p < 0.001$). The average protrusion width was 14.7 pixels in celiacs versus 13.9 pixels in controls ($p = 0.01$). The mean protrusion height was 3.10 ± 2.34 grayscale levels for celiacs versus 2.70 ± 0.43 grayscale levels for controls ($p < 0.001$). Thus celiac patients had significantly fewer protrusions on the luminal surface of the small intestine as compared with controls, and these protrusions had greater dimensions, suggesting they are indicative of a mosaic (cobblestone) macro-architectural pattern which is common in celiacs.

Conclusions: Shape-from-shading modeling is useful to explore luminal macro-architecture and to detect significant differences in luminal morphology in celiac versus normal patients, which can increase the usefulness of videocapsule studies.

* *Corresponding author at*: Harkness Pavilion 804, Columbia University, 180 Fort Washington Avenue, New York, NY 10032, USA. Tel.: +1 2123055447.
E-mail address: ciaccio@columbia.edu (E.J. Ciaccio).

0169-2607/$ – see front matter © 2013 Elsevier Ireland Ltd. All rights reserved.
http://dx.doi.org/10.1016/j.cmpb.2013.06.002

1. Background

The mucosal surface of the small intestine is characterized by folds and villi which are approximately 0.5 mm long and 0.1 mm in diameter in healthy human patients [1]. In health, epithelial cells lining the villi transport nutrients from the intestinal lumen to the bloodstream [2]. In celiac disease, as a result of an immune reaction to dietary gluten, the mucosa becomes inflamed and villi become shortened (villous atrophy), and malabsorption of nutrients occurs [3]. At the microscopic level, villous projections become small or nonexistent [3,4]. Endoscopically, the mucosal appearance has visible fissuring that frequently displays a mosaic or cobblestone appearance. The mucosal folds when viewed side-on may appear scalloped. These structural changes are likely to be reflected quantitatively as alterations in the three-dimensional mucosal architecture.

While endoscopic visualization of the small intestinal mucosal surface using video endoscopic techniques is the standard method of assessing the mucosal surface and allows biopsy for the diagnosis of celiac disease, other methods are also available. These include contrast-enhanced magnetic resonance (MR) imaging as a way to show the mucosal changes in celiac disease [5]. Another novel diagnostic technique is endocytoscopy, which enables real-time visualization of the intestinal mucosa at 450× magnification, so that intestinal villi dimensions can be determined [6]. Moreover, irregular and abnormal peristalsis is present in most untreated celiac patients and can be evaluated by means of ultrasound using a combination of signs [7]. Computed tomography can also be implemented to discriminate celiac disease from other maladies, but has thus far been limited to visual analyses [8]. Any imaging method to detect pathology throughout the small intestinal lumen in celiac patients should be able to assess not only the typical endoscopic markers including a reduction or absence of duodenal folds, scalloping of the duodenal folds, mosaic or cobblestone appearance of the mucosal surface, and mucosal fissures, crevices or grooves, but also to directly assess whether villous atrophy is present [9].

Videocapsule endoscopy can be used to acquire high-resolution images from the entire small intestinal mucosa [4,10,11]. In previous work, it was shown that differences in mucosal architecture related to villous atrophy can be detected by measuring videocapsule image texture [4,10,11]. Texture can be defined as the variation in image brightness at scales smaller than the region of interest, and can be measured as the standard deviation from the mean [12]. Using this measurement for comparison of celiac versus control videoclips, texture was found to be significantly greater in celiacs [4,10,11]. It was hypothesized that the increased texture was correlated to abnormal macroscopic image features, which are in turn related to villous atrophy at the microscopic level. However, this textural measurement is not indicative of the three-dimensional profile of mucosal architecture. If there were a way to encode for three-dimensional structure, it could be useful to detect additional features of abnormal mucosa. The shape-from-shading transformation from two to three dimensions can provide information regarding object depth, and it is useful for correction of tissue area estimates [13]. In the current study, we sought to construct a three-dimensional rendering of two-dimensional videocapsule images using shape-from-shading principles. This was done, as a first approximation, by linearly converting grayscale level to image depth. In so doing, abnormalities in celiac small intestinal mucosa could be measured as alterations in three-dimensional architecture. The objective of the study was to characterize the three-dimensional architecture of the small intestinal surface using a particular syntax, which as we shall show, is useful for distinguishing celiac from control videoclips.

1.1. *Acquisition and preprocessing of clinical data*

For quantitative analysis, videocapsule endoscopic images were obtained from patients who had provided informed consent prior to endoscopy. Indications for this procedure include suspected celiac disease, suspected Crohn's disease, obscure bleeding, iron-deficient anemia, and chronic diarrhea. Patients under 18 years of age, pregnant women, and those with a history of intestinal obstruction, presence of a pacemaker, or chronic use of non-steroidal anti-inflammatory drugs (NSAIDs) were excluded. Only complete videocapsule endoscopy studies, reaching the colon, were used for analysis. Retrospective analysis of videocapsule endoscopy data was approved by the Internal Review Board at Columbia University Medical Center.

The PillCamSB2 videocapsule (Given Imaging, Yoqneam, Israel) was used to obtain small bowel images. The system consists of a recorder unit, real-time viewer, battery pack, antenna lead set, recorder unit cradle and harness, battery charger, and real-time viewer cable. The capsule is 26 mm × 11 mm in size. A light source illuminates the luminal wall in line with the camera direction. All subjects swallowed the PillCam SB2 videocapsule with radio transmitter after a 12 h fast and wore a small portable recording device. The recorder received radioed images via a sensor array that was transmitted by the videocapsule as it passed through the GI tract. The procedure began in early morning by swallowing the capsule with approximately 200 ml of water, and investigation was terminated either upon arrival of the capsule in the cecum, or after 8 h. Subjects were allowed to drink water 2 h after ingesting the capsule, and to eat a light meal after 4 h. Videos were reviewed and interpreted by an experienced gastroenterologist using a HIPAA-compliant PC-based workstation equipped with Given Imaging analysis software that was also used to export videos for further analysis.

Retrospective data were obtained from 10 celiac patients on a regular diet or within 3 months of starting a gluten-free diet. In these patients the diagnostic biopsy revealed Marsh grade II–IIIC lesions [14]. All patients were evaluated at Columbia University Medical Center, New York, from May 1, 2008 to July 31, 2009. The celiac cohort consisted of 5 female and 5 male patients (mean ages 50.5 and 44.0 years, respectively), and a control group 6 female and 4 male patients (mean ages 50.0 and 51.5 years, respectively). The videocapsule frame rate was set to acquire two digital images per second with the image dimension being 576 × 576 pixels.

Videoclips obtained from four locations in the small intestine of each patient were analyzed retrospectively. The four regions were: (1) duodenal bulb, (2) distal duodenum, (3) jejunum, and (4) proximal ileum. The recorded digital information was downloaded to the computer console, and videos from the small and large bowel were reviewed using proprietary software. A sequence of 200 consecutive images (i.e., 100 s) was extracted from each videoclip for Matlab processing (ver. 7.7, The MathWorks, 2008, Natick, MA). The videocapsule endoscopic images of celiac patients that were used for analysis were taken from regions that appeared abnormal. Videocapsule endoscopic images were also obtained from 10 control patients. All image sequences used for analysis were selected to have minimal presence of extraneous substances such as air bubbles and opaque fluids. From the portions of each videoclip meeting these criteria at each small intestinal level, the 200 image sequence used for analysis was randomly extracted. The actual image resolution depended on the camera–lumen distance. The PillCam is 11 mm in length and has a field-of-view of 140°. Supposing that the PillCam is positioned vertically on the lumen surface so that the videocamera is oriented in the normal direction toward the surface on the opposite side, and that the lumen diameter is 25 mm, this maximum videocamera–lumen distance is 14 mm. From trigonometry, the camera viewing area would then be 7.5 cm × 7.5 cm, so that the minimum image resolution, for 256 × 256 pixel images, is approximately 0.2 mm. Each image obtained from the videoclip was initially in RGB color format. For simplicity in processing, the extracted images were converted to 256 grayscale levels (0 = black, 255 = white), resized to 576 × 576 pixels, and stored in Portable Gray Map (pgm) specification via a commercial software program (Matlab ver. R2009b, The MathWorks, Natick MA). The preprocessed images were viewed using the ImageJ software program [15].

2. Methods

2.1. Shape-from-shading transformation

The shape-from-shading problem is to compute a three-dimensional shape from a grayscale image [16]. Determining three-dimensional shape from grayscale shading is a problem that has no unique solution [16]. As a first approximation we suppose that the camera and light source are directed normal to and at constant distance from the luminal surface, so that there is a direct relationship between the reflectance map and image brightness [16]. Based upon the Inverse Square Law, regions closer to the camera lens and light source will be brighter in appearance. We used a linear approximation for the small imaging distances between camera and luminal wall, since these measurements are near the base of the parabola representing the inverse square function. The same treatment was applied to all data, so that any distortion imposed by this constraint was unbiased. Thus each videocapsule image was converted to a three-dimensional representation with dimensions: *x*–*y* (width and length in pixels) and depth (256 grayscale levels).

2.2. Syntactic analysis

Three-dimensional structures were characterized as follows using shape-from-shading principles. A syntax was developed to quantify three-dimensional macro-architecture. A protrusion was defined as a 9 × 9 pixel area with the center pixel having the greatest brightness of any of the 81 pixels in that area (see Fig. 1, asterisk). The values for model length × width of 9 × 9 pixels approximated the observed protrusion dimensions that were evident in videocapsule imagery. The protrusion location was defined by the *XY* coordinate of the center pixel in the kernel. This step was repeated by shifting the kernel across the entire image. The height and width of each detected protrusion were calculated as follows. The mean brightness within the 9 × 9 pixel area centered on each detected protrusion was calculated (square area within solid white line in Fig. 1). The average brightness level for all pixels along each successively larger concentric square was then calculated. The first such square is 11 pixels on each side and is marked in Fig. 1B. The total number of pixels contained within the square edges is:

$$(4 \times 11) - 4 = 40$$

For the next square which is 13 pixels on each side, the total number of pixels used for calculating mean brightness was:

$$(4 \times 13) - 4 = 48$$

The average pixel brightness within the 9 × 9 square edge, the 11 × 11 square edge, and so on, was plotted as shown near the bottom of Fig. 1B. For concentric squares that are more distant from the center, the average brightness decreases and reaches a minimum for the concentric square that is 17 pixels on a side. Protrusion width was defined as the dimension of the concentric square at a minimum brightness, which is 17 in Fig. 1B. To prevent scalloped edges from being detected as protrusions, the maximum protrusion width was set to 100 pixels. Protrusion height was defined as the difference in average brightness level for the 9 × 9 area at center versus the concentric square at minimum brightness. Thus the syntax for describing protrusions was developed to detect bright spots with progressively decreasing brightness away from their centers, approximated by a square shape.

The number of protrusions per image, and the mean protrusion width and height per image, were averaged over the 200 image sequence in each videoclip. Pooled videoclip measurements for celiacs versus controls were then compared.

2.3. Spatial derivative and statistics

To quantify spatial relationships in each image, the first spatial derivative *dv* of protrusion width and height was calculated as the mean absolute difference between the value at a particular location and that of its four nearest-neighbors:

$$dv_w = \frac{1}{4}\sum \mathrm{abs}(w_c - w_i) \quad \text{for } i = 1-4 \tag{1}$$

$$dv_h = \frac{1}{4}\sum \mathrm{abs}(h_c - h_i) \quad \text{for } i = 1-4 \tag{2}$$

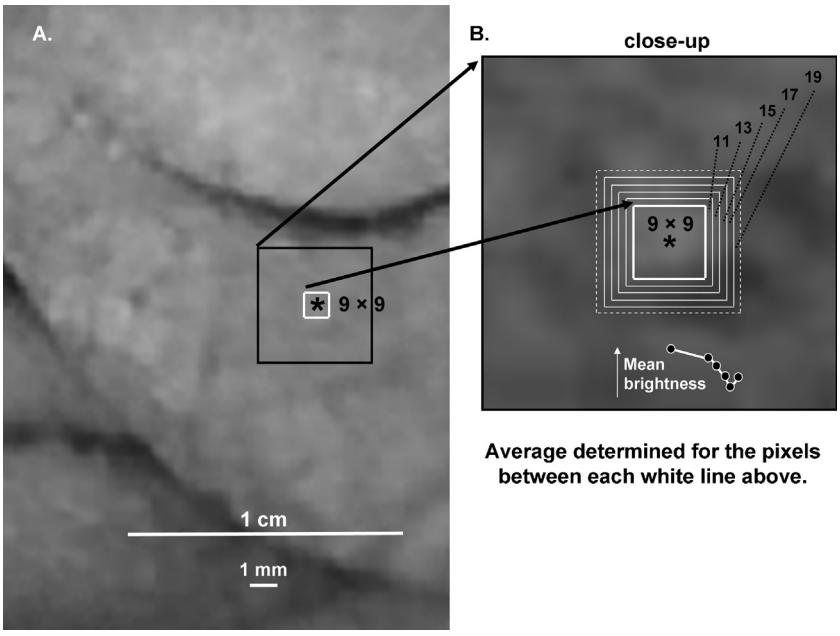

Fig. 1 – Schematic illustration of the macro-architectural model. Luminal surface protrusions were identified using a square edge. Although few protrusions were actually square in dimension, the measurement proved to be a good approximation (see Table 1).

where w_c is the width of a particular protrusion for which the spatial derivative is being calculated, w_i is the width of its four nearest-neighbors, h_c is the height of the particular protrusion, and h_i is the height of its four nearest-neighbors.

Using a fast PC-type computer, the above calculations were completed in approximately 1 min for each of the 200 frame sequences.

2.4. *Statistics*

The unpaired *t*-test and the *F* statistical test were used to determine significant differences in the means and standard deviations, respectively (SigmaPlot 2004 for Windows Ver. 9.01, Systat Software, MedCalc Statistical Software 2008, ver. 9.5 Belgium).

3. Results

An example of a two-dimensional image to three-dimensional rendering from a celiac patient videoclip, obtained at the level of the distal duodenum, is depicted in Fig. 2. Panel A shows the PillCam image prior to processing, one of 200 images per videoclip. Numerous mucosal folds with scalloping are observable, and there is a mosaic appearance. The smoothed three-dimensional rendering of this image is shown in Fig. 2B, oriented to better display the protrusions. This rendering (and those of Figs. 3–7) was done using map3d, an interactive scientific visualization tool for bioengineering data (Scientific Computing and Imaging Institute, University of Utah) [17]. For clarity, the three-dimensional location of each pixel/grayscale level was shown at half-resolution (decimation

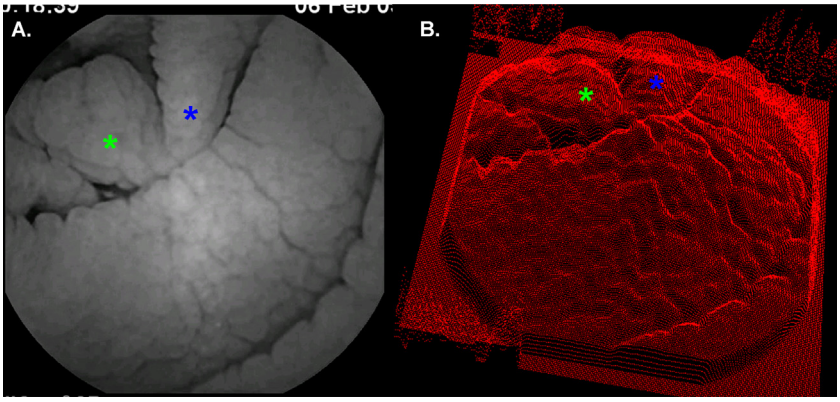

Fig. 2 – Example of (A) two-dimensional image and (B) three-dimensional rendering, celiac patient data. Darker areas in (A) are represented by lower elevations in (B). Around the three-dimensional image representation in (B), grayscale level 0 (black) is shown for reference (planar region at edges); same for Fig. 5.

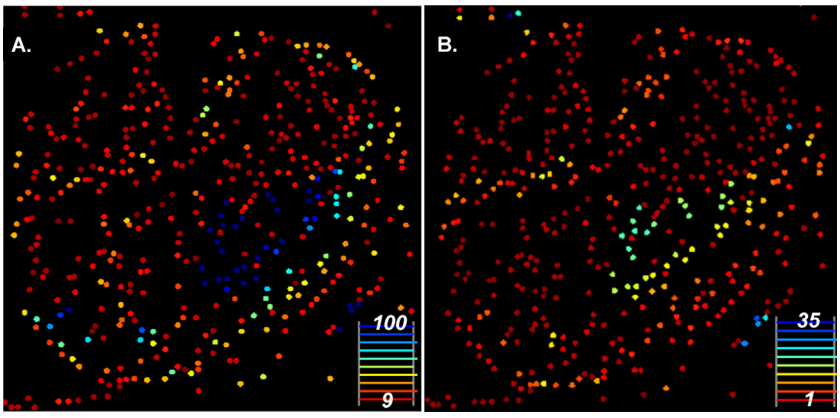

Fig. 3 – Example of protrusion measurement for celiac patient data (same image as Fig. 2). The detected protrusions are denoted as circles. For clarity, the total number of detected protrusions was subsampled to generate the maps. (A) Width – protrusions with maximal width are evident at center right (blue). (B) Height – protrusions with maximal height are also evident at center right (blue). The largest protrusions detected correspond with those evident in Fig. 2. Scalloped edges are too large to appear as protrusions. (For interpretation of the references to color in this figure legend, the reader is referred to the web version of this article.)

by two) after application of the smoothing kernel. The baseline level is evident at the edges in Fig. 2B with extraneous lettering appearing as tall peaks at some of the corners. Features of the two-dimensional shading in panel A are represented as three-dimensional structures in panel B. For example, selected corresponding locations are shown by colored asterisks in panels A and B.

Locations of luminal protrusions from Fig. 2 that were detected by the concentric squares macro-architectural model are noted as circular points in Fig. 3A. The color scale denotes protrusion width from smaller (red) to larger (blue) with 100 being the maximum as noted in Section 2. Many of the protrusion widths are wide (blue) or intermediate (yellow) at the area where the mosaic pattern is the most evident (compare Fig. 3A with Fig. 2). The scale for protrusion width is given at lower right in units of pixels. In Fig. 3B the result is shown for the protrusion height calculations using the same image. As in Fig. 3A, in Fig. 3B the locations of the protrusions are noted as circles. The color scale from red to blue indicates greater protrusion height. It is evident that protrusions with greater height (panel B) tend to have greater width as well (panel A). The scale for protrusion height is given at lower right in the panel, and it ranges to a maximum of 35 grayscale level units.

Corresponding histograms for the protrusion width and height maps of Fig. 3 are shown in Fig. 4. The width bin from 0 to 9 represents protrusions with widths of only 9 pixels. The

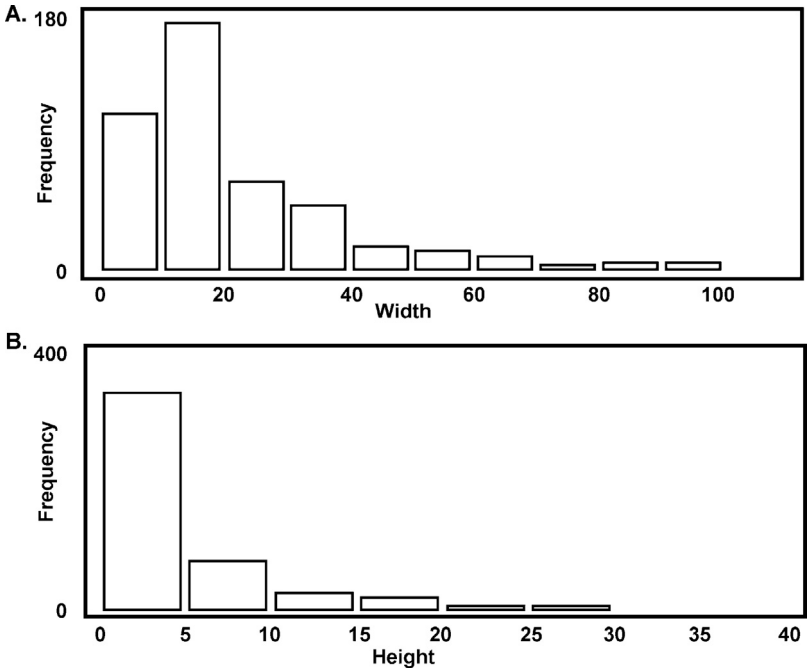

Fig. 4 – Histograms of the frequency of protrusion width (A) and height (B) for the corresponding maps in Fig. 3.

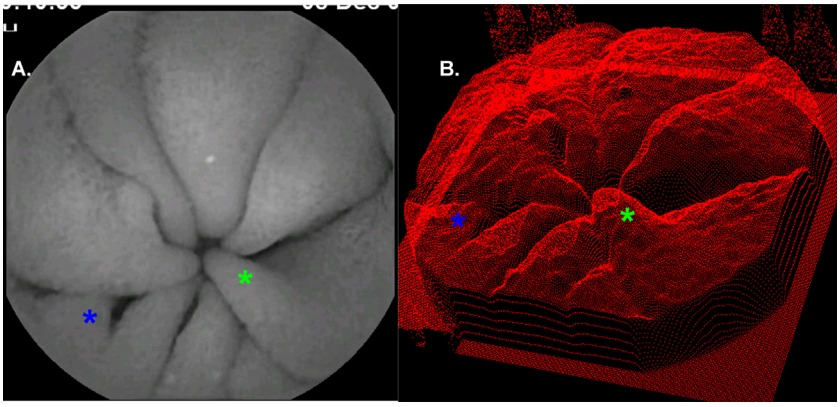

Fig. 5 – Example of two-dimensional image and three-dimensional rendering from a control patient.

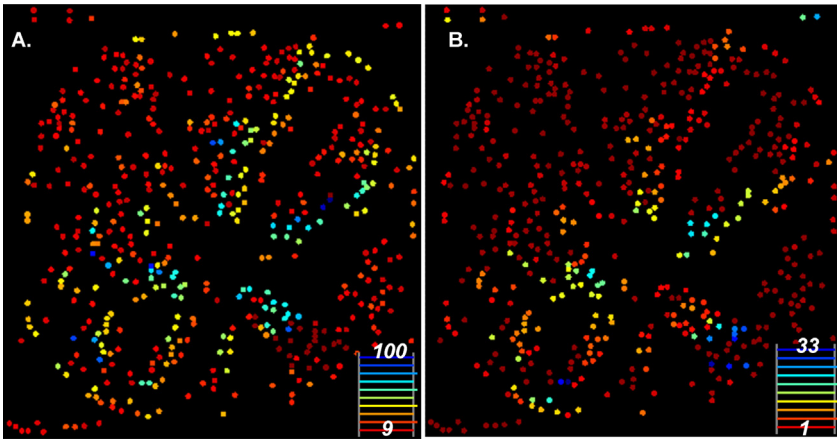

Fig. 6 – Example of protrusion measurement for a control patient image (same image as Fig. 5). The detected protrusions are shown as circles. For clarity, the total number of detected protrusions was subsampled to generate the maps. (A) Width – protrusions with maximal width are seldom evident (blue). (B) Height – protrusions with maximal height are noted in blue. (For interpretation of the references to color in this figure legend, the reader is referred to the web version of this article.)

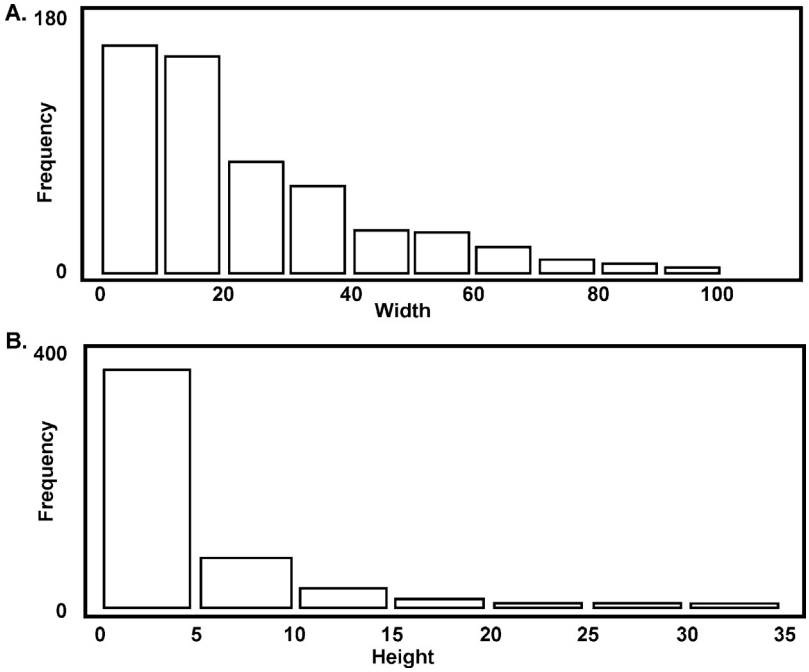

Fig. 7 – Histograms of the frequency of protrusion width (A) and height (B) for the corresponding maps in Fig. 6. Both the width and the height measurement tend to cluster at lower values.

bin with the most pixels is at width 10–19. Both the width and the height measurement tend to spread toward higher values.

An example of two-dimensional imaging and three-dimensional rendering from a control patient is shown in Fig. 5. Panel A shows the PillCam image which was obtained from the distal duodenum. Several folds are evident (panel A). Other than for the folds, the image is mostly uniform across the luminal surface as compared with the celiac image of Fig. 2A. The three-dimensional rendering is shown in Fig. 5B. Some corresponding areas are noted by asterisks. Protrusions are evident but they appear small and uniform as compared with those of the celiac image in Fig. 2B. In Fig. 5B, lettering in the PillCam image appears as artifact at the top. The edges of the image are shown as flat surfaces.

Locations of luminal protrusions from Fig. 5 that were detected by the concentric squares macro-architectural model are noted as circular points in Fig. 6A. The color scale denotes protrusion width from smaller (red) to larger (blue) with 100 being the maximum possible value. Only a few protrusions are wide (blue color) as compared with Fig. 3A. Most protrusions are narrow (red color). In Fig. 6B the result is shown for the protrusion height calculation using the same image. As in Fig. 6A, in Fig. 6B protrusion locations are noted by circles. The color scale from red to blue indicates greater protrusion height. Taller protrusions are mostly confined to a small region at center.

Corresponding histograms for the protrusion width and height maps are shown in Fig. 7. Both the width and the height measurement tend to be clustered at lower values as compared with the corresponding histograms for the celiac patients shown in Fig. 4. For the protrusion width histogram (Fig. 7A) the maximum frequency occurs at the narrowest width, unlike the corresponding histogram for the celiac patient in Fig. 4A. The protrusion heights cluster at lower values for the control patient (Fig. 7B) as compared with the celiac patient (Fig. 4B). Thus most of the protrusions in this control patient image are small and uniform as compared with the celiac patient image.

3.1. *Summary statistics*

Results for all patients are summarized in Table 1. Shown from top to bottom rows are the mean number of protrusions per image, mean and standard deviation of protrusion width in pixels, the mean spatial derivative in protrusion width, mean and standard deviation of protrusion height above baseline level (grayscale units), and spatial derivative in protrusion height. Most differences between celiacs and controls are highly significant. The celiacs have more protrusions per image than celiacs, and these are greater in mean width and height, and have larger spatial derivatives in width and height as compared with controls. There is greater uniformity in size in terms of protrusion width and height in controls (lesser standard deviation, which is significant for the height measurement). Thus control patients tend to exhibit more uniform protrusions throughout the luminal surface (lesser spatial derivative), while celiac patients tend to have larger, irregularly sized protrusions.

4. Discussion

In this study, a syntax, which is a quantitative description of the way in which structural elements are arranged, was developed to quantify the morphology of small intestinal protrusions as evidenced by videocapsule imaging data. The results indicate that the model syntax, described in Section 2, is useful to distinguish mosaic pattern in celiac patient videocapsule images (Figs. 2–4) as compared to the more uniform and fine texture in control patient images (Figs. 5–7). Overall, significant differences between celiacs and controls were found in most parameters, as would be expected due to the presence of villous atrophy in celiac patients. In this study only macro-architectural protrusions were quantified, with dimensions on the order of a few millimeters. In future studies the syntax could be revised to describe fissures or scalloping that are also often present in untreated or recently treated celiac patients, as well as in those patients who are refractory to the gluten-free diet. Thus there is the potential for the method to assist in diagnosis and treatment.

4.1. *Quantitative measurement of the small intestinal mucosa from endoscopic images*

Other investigators have used differing approaches to quantify the small intestinal mucosal surface from endoscopic images. Shape-from-shading endoscopic investigation has also been implemented using formulae for irradiance and photometric calibration [18]. Other algorithms for quantification consider the close proximity of light source to luminal wall [19]. Such algorithms can be used to discriminate pathology from normal duodenum [20]. It is also possible to evaluate the quantitative

Table 1 – Statistical results of luminal protrusion measurements.

Measurement	Celiac	Control	Significance
# Protrusions/image	402.21 ± 14.99	420.79 ± 23.97	$p < 0.001$
Protrusion width MN	14.66 ± 1.04	13.91 ± 1.47	$p = 0.01$
Protrusion width SD	20.96 ± 2.34	20.53 ± 3.40	NS
Protrusion width dv_w	12.38 ± 1.01	11.93 ± 0.95	$p < 0.05$
Protrusion height MN	3.10 ± 0.26	2.70 ± 0.43	$p < 0.001$
Protrusion height SD	6.20 ± 0.42	5.75 ± 0.55	$p < 0.001$
Protrusion height dv_h	3.06 ± 0.32	2.69 ± 0.40	$p < 0.001$

Width in pixels; height in grayscale level; MN, mean; SD, standard deviation; NS, not significant; dv, spatial derivative.

results from a series of endoscopic images so as to map the mucosal surface in real-time on a computerized grid [21]. Thus other investigators have found it possible to use endoscopic imagery successfully for detection of celiac disease features.

4.2. *Clinical correlates*

There is a need to model the macro-architecture of the small intestinal luminal surface when villous atrophy is present to differentiate celiac videocapsule images from normal images. Our study was an initial attempt to model the luminal surface at the level of resolution of videocapsule imagery (on the order of millimeters). Differences in three-dimensional architecture of the small intestinal mucosal surface between celiacs and controls, according to the syntax devised in this study, was for the most part highly significant (Table 1). Since macro-architecture on the order of millimeters was quantified, it suggests that the increased height and width of celiac protrusions, and their more spatially varied form, is a manifestation of the frequently present mosaic or cobblestone appearance of the intestinal mucosa in these patients. Thus we believe that the technique will be useful to detect and map areas of villous atrophy in a prospective series of celiac patients, as planned for future study. Other syntaxes can be devised for describing protrusions and other features of the small intestinal lumen including the fissures that are commonly present in celiac patient intestinal mucosa due to pathology, and the scalloping of mucosal folds [22,23]. In the case of fissures for example, rather than protrusions the goal would be to detect small grooves or valleys in the mucosal surface that can be linear or curved. These features are similar in scale to the protrusions. On a larger scale, detection of scalloping of mucosal folds will first require the development of a syntactic definition of the mucosal folds themselves, and then discriminating normal folds from scalloped ones.

Based on this analysis, a mapped profile of the state of the villi could be developed along the entire small intestine. We would expect that, as celiac disease is known to have patchy areas of villous atrophy [3] there will be areas with little or no atrophy according to the morphologic measurements, as well as areas with severe atrophy. Areas lacking atrophy in celiacs would be expected to have lesser quantitative macro-architectural difference as compared with normal small intestinal mucosa. As atrophy becomes more severe, the change in profile can be measured quantitatively, even at the light microscopic level [24], suggesting that the macro-architecture that is resolvable at this level of resolution is altered, as also found in our study.

Small intestinal regions with villous atrophy are patchy in celiac disease, which would be expected to be manifested as patchy regions of macro-architectural change on the order of the few millimeters resolution that was used for quantification in our study. Thus would be expected larger spatial derivatives in protrusion width and height in celiacs, as was observed (Table 1). In contrast, our syntax suggested that control patients have a more uniform, carpet-like macro-architectural appearance of the small-intestinal lumen.

Another investigation has shown that Bayesian and support vector machines can be useful to segment the gastrointestinal tract according to four major topographic areas: the entrance, stomach, small intestine, and large intestine, which is used to reduce manual annotation time [25]. Automatic diagnosis of intestinal motility diseases (as in celiacs who tend to have reduced motility) [21,26,27] using video capsule endoscopy is also possible [28]. Thus a further use of our syntax would be for application to image frames in real time so that changes in three-dimensional architecture can be correlated to luminal location and to motility. Moreover, this algorithm could be applied to celiac patients beginning a gluten free diet, to monitor the effectiveness of the diet, and to map changes along the small intestine during recovery.

4.3. *Conclusions*

Videocapsule endoscopy images of the small intestinal lumen were converted to three-dimensional macro-architectural structures using shape-from-shading principles. A syntax was developed to describe, compare, and contrast this three-dimensional morphology in celiac patients versus controls. It was found that significant differences in morphology exist between celiacs and controls. Notably, in celiacs the luminal protrusions are less spatially uniform, and are taller in height and wider in width which is a likely manifestation of the patchy, mosaic or cobblestone appearance. The method is therefore potentially useful to detect pathologic areas of the small intestine in celiacs during real-time capsule endoscopy, as well as to monitor the efficacy of a gluten-free diet.

4.4. *Limitations*

For simplicity, presence of opaque materials within the luminal fluid was treated as random noise that would not significantly affect significant differences in the three-dimensional architecture between celiac and control patients. A method has been devised by other investigators to remove extraneous information from videocapsule images [20], which could be incorporated into future versions of our algorithm. The effects of light reflection and proximity of the luminal surface to the camera lens were considered, as a first approximation, to equally affect celiac and control images. These extraneous influences may result in slightly reduced significance between the two populations of patients. The statistical population was relatively small in this pilot study ($N = 10$ celiacs and $N = 10$ control subjects, 4 small intestinal levels in each). Thus results should be confirmed in a larger pool of subjects prior to planning a clinical trial. Our results were pooled from all videoclips without regard to small intestinal location. By separating the videoclip measurements based upon location, in a study with a larger population of patient data, it will be possible to characterize differences in the three-dimensional morphology of the small intestinal lumen according to anatomic location. This may be important, for example, to characterize the healing process along all portions of the small intestinal lumen in celiacs after onset of the gluten-free diet (duodenal bulb, distal duodenum, jejunum, and ileum), as well as to determine whether the profile of villous atrophy differs markedly between celiac patients according to age, gender, and presence of refractory disease.

Conflicts of interest statement

We declare that we have no conflicts of interest.

Acknowledgments

The implementation of this study was made possible in part with a grant from the Celiac Sprue Association Peer Review Research Grant Program. Figs. 3 and 6 were created using software from the NIH/NCRR Center for Integrative Biomedical Computing, P41-RR12553-10.

REFERENCES

[1] M. Hasan, A. Ferguson, Measurements of intestinal villi in non-specific and ulcer-associated duodenitis correlation between area of microdissected villus and villus epithelial cell count, J. Clin. Pathol. 34 (1981) 1181–1186.
[2] B.M. Koeppen, B.A. Stanton, Physiology, Mosby Company, Saint Louis, 2009, pp. 718–744.
[3] P.H.R. Green, C. Cellier, Celiac disease, N. Engl. J. Med. 357 (2007) 1731–1743.
[4] E.J. Ciaccio, G. Bhagat, C.A. Tennyson, S.K. Lewis, L. Hernandez, P.H. Green, Quantitative assessment of endoscopic images for degree of villous atrophy in celiac disease, Dig. Dis. Sci. 56 (2011) 805–811.
[5] G. Masselli, A. Picarelli, M. Di Tola, V. Libanori, G. Donato, E. Polettini, A. Piermattei, P. Palumbo, A. Pittalis, A. Saponara, G. Gualdi, Celiac disease: evaluation with dynamic contrast-enhanced MR imaging, Radiology 256 (2010) 783–790.
[6] T. Matysiak-Budnik, E. Coron, J.F. Mosnier, M. Le Rhun, H. Inoue, J.P. Galmiche1, In vivo real-time imaging of human duodenal mucosal structures in celiac disease using endocytoscopy, Endoscopy 42 (2010) 191–196.
[7] D. Bartusek, V. Valek, J. Husty, J. Uteseny, Small bowel ultrasound in patients with celiac disease, Eur. J. Radiol. 63 (2007) 302–306.
[8] M. Mallant, M. Hadithi, A.B. Al-Toma, M. Kater, M. Jacobs, R. Manoliu, C. Mulder, J.H. van Waesberghe, Abdominal computed tomography in refractory celiac disease and enteropathy associated T-cell lymphoma, World J. Gastroenterol. 13 (2007) 1696–1700.
[9] G. Cammarota, P. Fedeli, A. Gasbarrini, Emerging technologies in upper gastrointestinal endoscopy and celiac disease, Nat. Clin. Pract. Gastroenterol. Hepatol. 6 (2009) 47–56.
[10] E.J. Ciaccio, C.A. Tennyson, G. Bhagat, S.K. Lewis, P.H. Green, Classification of videocapsule endoscopy image patterns: comparative analysis between patients with celiac disease and normal individuals, BioMed. Eng. Online 9 (2010) 44.
[11] E.J. Ciaccio, C.A. Tennyson, S.K. Lewis, S. Krishnareddy, G. Bhagat, P.H. Green, Distinguishing patients with celiac disease by quantitative analysis of videocapsule endoscopy images, Comput. Methods Prog. Biomed. 100 (2010) 39–48.
[12] T.M. Deserno (Ed.), Biomedical Image Processing, Springer, New York, 2011, p. 157.
[13] B.L. Craine, E.R. Craine, C.J. O'Toole, Q. Ji, Digital imaging colposcopycorrected area measurements using shape-from-shading, IEEE Trans. Med. Imaging 17 (1998) 1003–1010.
[14] M.N. Marsh, Gluten: major histocompatibility complex and the small intestine: a molecular and immunobiologic approach to the spectrum of gluten sensitivity ('celiac sprue'), Gastroenterology 102 (1992) 330–354.
[15] W.S. Rasband, ImageJ, U.S. National Institutes of Health, Bethesda, MA, USA, 1997–2012 http://imagej.nih.gov/ij/
[16] E. Prados, O. Faugeras, Shape from shading, in: Handbook of Mathematical Models in Computer Vision, Springer, New York, 2005, pp. 375–388.
[17] R.S. MacLeod, C.R. Johnson, Map3d: interactive scientific visualization for bioengineering data:, in: IEEE Engineering in Medicine and Biology Society 15th Annual International Conference, IEEE Press, New York, 1993, pp. 30–31.
[18] C. Wu, S.G. Narasimhany, B. Jaramazy, Shape-from-shading under near point lighting and partial views for orthopedic endoscopy, in: Workshop on Photometric Analysis For Computer Vision, October 14–21, Rio de Janeiro, Brazil, 2007.
[19] T. Okatani, K. Deguchi, Shape reconstruction from an endoscope image by shape from shading technique for a point light source at the projection center, Comput. Vision Image Understand. 66 (1997) 119–131.
[20] L. Igual, J. Vitrià, F. Vilariño, S. Seguí, C. Malagelada, F. Azpiroz, P. Radeva, Automatic discrimination of duodenum in wireless capsule video endoscopy, in: 4th European Conference of the International Federation for Medical and Biological Engineering, pp 1536–1539. IFMBE Proceedings Volume 22, Part 11, 2009.
[21] S. Seshamani, W. Lau, G. Hager, Real-time endoscopic mosaicking:Me, Image Comput. Comput. Assist. Interv. 9 (Pt 1) (2006) 355–363.
[22] P.H. Green, B. Jabri, Coeliac disease, Lancet 362 (2003) 383–391.
[23] P.H. Green, Mortality in celiac disease: intestinal inflammation and gluten sensitivity, JAMA 302 (2009) 1225–1226.
[24] E.J. Ciaccio, G. Bhagat, C.A. Tennyson, S.K. Lewis, L. Hernandez, P.H. Green, Quantitative assessment of the degree of villous atrophy in patients with coeliac disease, J. Clin. Pathol. 61 (2008) 1089–1093.
[25] J.S. Cunha, M. Coimbra, P. Campos, J.M. Soares, Automated topographic segmentation and transit time estimation in endoscopic capsule exams, IEEE Trans. Med. Imaging 27 (2008) 19–27.
[26] S. Cucchiara, G. Bassotti, G. Castellucci, R. Minella, C. Betti, C. Fusaro, A. Morelli, A. Bertotto, S. Auricchio, Upper gastrointestinal motor abnormalities in children with active celiac disease, J. Pediatr. Gastroenterol. Nutr. 21 (1995) 435–442.
[27] L. Elli, M.T. Bardella, Motility disorders in patients with celiac disease, Scand. J. Gastroenterol. 40 (2005) 743–749.
[28] F. Vilarino, P. Spyridonos, F. Deiorio, J. Vitria, F. Azpiroz, P. Radeva, Intestinal motility assessment with video capsule endoscopy: automatic annotation of phasic intestinal contractions, IEEE Trans. Med. Imaging 29 (2010) 246–259.